Hindawi Publishing Corporation
Journal of Atomic, Molecular, and Optical Physics
Volume 2012, Article ID 916510, 11 pages
doi:10.1155/2012/916510

Research Article

Electronic-Rotational Coupling in Cl–*para*-H_2 Van der Waals Dimers

Robert J. Hinde

Department of Chemistry, University of Tennessee, Knoxville, TN 37996-1600, USA

Correspondence should be addressed to Robert J. Hinde, rhinde@utk.edu

Received 31 July 2012; Accepted 12 November 2012

Academic Editor: Hari P. Saha

We examine the interaction between an open-shell chlorine atom and a *para*-H_2 molecule in the region of configuration space that corresponds to a weakly bound Cl–*para*-H_2 van der Waals dimer. By constructing and diagonalizing the Hamiltonian matrix that represents the coupled Cl atom electronic and H_2 rotational degrees of freedom, we obtain one-dimensional energy curves for the Cl–*para*-H_2 system in this region of configuration space. We find that the dimer exhibits fairly strong electronic-rotational coupling when the Cl–H_2 distance R is close to $R = 5.5a_0$; however, this coupling does not modify substantially the positions and depths of the van der Waals wells in the dimer's $E(R)$ curves. An approximation in which the *para*-H_2 fragment is treated in the strict $j = 0$ limit thus appears to yield an accurate representation of those states of the weakly bound Cl–*para*-H_2 dimer that correlate with $j = 0$ H_2 in the $R \to \infty$ limit.

1. Introduction

Experimental studies [1] of the infrared absorption spectra of solid *para*-H_2 matrices that contain chlorine atoms as substitutional impurities indicate that Cl–H_2 interactions raise the transition energy associated with the $^2P_{1/2} \leftarrow {}^2P_{3/2}$ spin-orbit (SO) transitions of the Cl impurities. In these systems, the H_2 molecules in the Cl atom's first "solvation shell" reside in the van der Waals region of the Cl–H_2 potential energy surface [2]. A detailed analysis of the matrix-induced blue shift of the SO transition for Cl atoms embedded in solid *para*-H_2 would thus provide insight into the shape of the Cl–H_2 potential energy surface in this region of configuration space. This in turn could help us better understand the dynamics of the Cl + H_2 $\to$ HCl + H reaction, which has long been considered a benchmark system in chemical reaction dynamics [3]. For example, theoretical studies [4] of the HCl/DCl product branching ratio of the Cl + HD reaction suggest that the van der Waals region of the potential energy surface plays a key role in controlling the reaction's dynamics at low collision energies.

In the *para*-H_2 matrix, the Cl atom's SO transition is blue shifted by about 60 cm^{-1} by Cl–H_2 interactions [1], which amounts to a shift of about 5 cm^{-1} for each of the twelve H_2 molecules in the Cl atom's first solvation shell. The matrix-induced blue shift of the Cl SO transition can be qualitatively understood as arising from subtle differences in the van der Waals interactions of the ground and excited SO states of the Cl atom with nearby H_2 molecules. For a simulation to reproduce quantitatively the observed blue shift, we might therefore anticipate that the potential energy surfaces used in the simulation should be accurate to better than 1 cm^{-1}. Theoretical studies of the matrix-induced shift would thus represent a fairly stringent test of the Cl–H_2 potential energy surfaces involving both the ground and excited SO states of the Cl atom.

Previous simulations [5, 6] of open-shell atomic impurities in *para*-H_2 matrices have employed a simplified model for the *para*-H_2 matrix, a model in which the H_2 molecules are treated as spherical particles. This is equivalent to assuming that the H_2 molecules in the matrix remain in the pure $j = 0$ ground rotational state, with their orientational degrees of freedom completely unperturbed by anisotropic interactions with the open-shell impurity. However, a careful study of the B-H_2 and Al-H_2 van der Waals dimers [7] indicated that the binding energies of these dimers increased

by 15% to 20% (or several cm^{-1}) when the $j = 0$ restriction for the H_2 monomer was relaxed and $j > 0$ rotational states were allowed to mix into the H_2 molecule's rotational wave function. Similar behavior in the Cl–H_2 dimer might raise concerns that the effective Cl–H_2 potential energy functions obtained from a pure $j = 0$ approximation for the H_2 molecule would be insufficiently accurate for a quantitative study of the matrix-induced blue shift of the Cl SO transition. In such a case, more sophisticated treatments [8] of the H_2 molecules' rotational degrees of freedom might be needed.

In this work, we examine electronic-rotational coupling in the Cl–*para*-H_2 van der Waals dimer, using the potential energy surfaces for the dimer presented in [9] as the foundation for our study. We find some evidence for moderately strong electronic-rotational coupling in the low-energy repulsive region of the Cl–H_2 potential energy surface. This coupling does not, however, substantially change the positions or depths of the van der Waals minima for dimers composed of a Cl atom and a *para*-H_2 molecule. This suggests that treating the H_2 molecules in Cl-doped solid *para*-H_2 as pure $j = 0$ molecules should be a reasonably good approximation.

2. Spin-Orbit States of an Isolated Cl Atom

We begin our investigation by reviewing the effects of SO coupling in an isolated chlorine atom. We first construct a basis set of antisymmetrized many-electron functions for the atom's $3p$ subshell; we will use this basis set to evaluate the matrix elements of the atom's effective SO operator. For future convenience, we choose these antisymmetrized many-electron functions to be Slater determinants of Cartesian $3p$ spin-orbitals in a space-fixed coordinate system. We use p_x and $\overline{p}_x$, respectively, to represent a one-electron Cartesian p_x orbital paired with either the spin-up or spin-down electron spin function. For specificity, we note that the p_x function is positive along the positive x axis. The six many-electron functions that span the subspace of interest are these Slater determinants:

$$P_x = (5!)^{-1/2} \det \left| p_x p_y \overline{p}_y p_z \overline{p}_z \right| \tag{1}$$

$$P_y = (5!)^{-1/2} \det \left| p_x \overline{p}_x p_y p_z \overline{p}_z \right| \tag{2}$$

$$P_z = (5!)^{-1/2} \det \left| p_x \overline{p}_x p_y \overline{p}_y p_z \right| \tag{3}$$

$$\overline{P}_x = (5!)^{-1/2} \det \left| \overline{p}_x p_y \overline{p}_y p_z \overline{p}_z \right| \tag{4}$$

$$\overline{P}_y = (5!)^{-1/2} \det \left| p_x \overline{p}_x \overline{p}_y p_z \overline{p}_z \right| \tag{5}$$

$$\overline{P}_z = (5!)^{-1/2} \det \left| p_x \overline{p}_x p_y \overline{p}_y \overline{p}_z \right|. \tag{6}$$

The Cl atom's SO operator is written as

$$\hat{V}_{\mathrm{SO}} = \left(\frac{C_{\mathrm{SO}}}{\hbar^2} \right) \times \hat{\mathbf{L}} \cdot \hat{\mathbf{S}}, \tag{7}$$

where $\hat{\mathbf{L}}$ and $\hat{\mathbf{S}}$ are the total orbital and spin angular momentum operators for the five electrons in the $3p$ subshell and the constant C_{SO} is two-thirds of the energy gap between the lower and upper SO energy levels of the Cl atom; this energy gap is $\Delta E_{\mathrm{SO}} = 882.35\,\mathrm{cm}^{-1}$ [10]. In a basis set consisting of these six Slater determinants, $\hat{V}_{\mathrm{SO}}$ has the matrix representation

$$V_{\mathrm{SO}} = C_{\mathrm{SO}} \times \begin{pmatrix} 0 & i/2 & 0 & 0 & 0 & -1/2 \\ -i/2 & 0 & 0 & 0 & 0 & i/2 \\ 0 & 0 & 0 & 1/2 & -i/2 & 0 \\ 0 & 0 & 1/2 & 0 & -i/2 & 0 \\ 0 & 0 & i/2 & i/2 & 0 & 0 \\ -1/2 & -i/2 & 0 & 0 & 0 & 0 \end{pmatrix}, \tag{8}$$

where the basis set is ordered $\{P_x, P_y, P_z, \overline{P}_x, \overline{P}_y, \overline{P}_z\}$ from left to right (and top to bottom). In the same basis set, the operator corresponding to the z-axis projection of the total angular momentum of the $3p$ subshell,

$$\hat{J}_z = \hat{L}_z + \hat{S}_z, \tag{9}$$

has the matrix representation

$$J_z = \hbar \times \begin{pmatrix} 1/2 & -i & 0 & 0 & 0 & 0 \\ i & 1/2 & 0 & 0 & 0 & 0 \\ 0 & 0 & 1/2 & 0 & 0 & 0 \\ 0 & 0 & 0 & -1/2 & -i & 0 \\ 0 & 0 & 0 & i & -1/2 & 0 \\ 0 & 0 & 0 & 0 & 0 & -1/2 \end{pmatrix}. \tag{10}$$

Because $\hat{V}_{\mathrm{SO}}$ and $\hat{J}_z$ commute with one another, we can simultaneously diagonalize the V_{SO} and J_z matrices. The normalized many-electron functions that do this are

$$\psi_{g,+3/2} = \frac{\left(-iP_x + P_y\right)}{\sqrt{2}} \tag{11}$$

$$\psi_{g,+1/2} = \frac{\left(2P_z - \overline{P}_x - i\overline{P}_y\right)}{\sqrt{6}} \tag{12}$$

$$\psi_{g,-1/2} = \frac{\left(iP_x + P_y + 2i\overline{P}_z\right)}{\sqrt{6}} \tag{13}$$

$$\psi_{g,-3/2} = \frac{\left(i\overline{P}_x + \overline{P}_y\right)}{\sqrt{2}} \tag{14}$$

$$\psi_{e,+1/2} = \frac{\left(P_z + \overline{P}_x + i\overline{P}_y\right)}{\sqrt{3}} \tag{15}$$

$$\psi_{e,-1/2} = \frac{\left(iP_x + P_y - i\overline{P}_z\right)}{\sqrt{3}}. \tag{16}$$

The four functions labeled with the subscript g are degenerate, with energy $E = -C_{\mathrm{SO}}/2$. They represent the four components of the Cl atom's $^2P_{3/2}$ lower SO energy level; the fraction listed in each function's subscript, when multiplied by $\hbar$, gives that function's $\hat{J}_z$ eigenvalue. The two functions labeled with the subscript e are degenerate components of the Cl atom's $^2P_{1/2}$ upper SO energy level and have energy $E = C_{\mathrm{SO}}$; these functions have $\hat{J}_z$ eigenvalues of $\pm\hbar/2$, as indicated

by their respective subscripts. Later, we will use the symbol j_z to represent the subscripts attached to the six many-electron SO wave functions listed above; the $\hat{J}_z$ eigenvalue for each function is thus $\hbar j_z$.

Next we examine the charge densities associated with the Cl atom's lower and upper SO energy levels. The charge density ρ associated with one of the six electronic wave functions ψ listed above is obtained by forming the product $|\psi|^2 = \psi^*\psi$, integrating over the five electrons' spin coordinates and the spatial coordinates of four of the five electrons, and multiplying by five. The final multiplication by five accounts for the fact that the many-electron function ψ is normalized so that integrating $|\psi|^2$ over all five electrons' spatial coordinates gives the value one, while integrating the charge density ρ over all space should give the value five.

To emphasize the shapes of these charge densities, we note that the charge density associated with the Slater determinant P_q, which corresponds to a singly occupied p orbital aligned with the space-fixed q Cartesian axis and doubly occupied p orbitals aligned with the other two space-fixed Cartesian axes, can be pictured as a $|p_q|^2$ charge density "hole" superimposed on the isotropic charge density function associated with a filled six-electron $3p$ subshell. We will represent this hole-plus-filled-subshell charge distribution using the symbol $H(p_q)$.

After computing the charge densities associated with the six SO wave functions listed above and writing them in terms of this symbol, we obtain

$$\rho_{g,\pm 3/2} = \frac{\left[H(p_x) + H\left(p_y\right)\right]}{2} \tag{17}$$

$$\rho_{g,\pm 1/2} = \frac{\left[H(p_x) + H\left(p_y\right) + 4H(p_z)\right]}{6} \tag{18}$$

$$\rho_{e,\pm 1/2} = \frac{\left[H(p_x) + H\left(p_y\right) + H(p_z)\right]}{3}. \tag{19}$$

This shows that the Cl atom's upper SO energy level has an isotropic charge density distribution, while the charge densities associated with the lower SO energy level are anisotropic. The $\psi_{g,\pm 3/2}$ wave functions have higher levels of electron density along the space-fixed Cartesian z-axis and lower levels of electron density in the (x, y) plane; the situation is reversed for the $\psi_{g,\pm 1/2}$ wave functions.

3. Cl–H_2 without Spin-Orbit Coupling

Now we consider a Cl–H_2 dimer in which the Cl atom is located at the origin of the space-fixed (x, y, z) coordinate system and the H_2 center of mass is located on the positive space-fixed z axis. We use α and β to represent the polar and azimuthal angles, respectively, of the H–H covalent bond in the space-fixed (x, y, z) coordinate system. The H–H covalent bond length is denoted r, and R is the Cl–H_2 distance. In this section, we neglect the effect of SO coupling in the Cl atom.

3.1. Characteristics of the Cl–H_2 Potential Energy Surface. First we set the azimuthal angle to $\beta = 0$, so that the H_2 molecule resides in the (x, z) plane. If we neglect effects related to SO coupling, then there are three Cl–H_2 adiabatic electronic states, each of which is doubly degenerate because of the spin-1/2 nature of the Cl–H_2 dimer [2, 9, 11]. Two of these states have A' spatial symmetry with respect to the (x, z) plane; these are states in which the p-orbital "hole" of the Cl atom resides in the (x, z) plane. The third state has A'' spatial symmetry; in this state, the Cl atom's p-orbital hole is aligned with the y-axis.

The two A' adiabatic electronic states, which we label $1A'$ and $2A'$ in order of increasing energy, can be viewed as linear combinations of diabatic states associated with the Slater determinants P_x and P_z. The mixing angle θ defines these linear combinations [2, 9, 11]:

$$\left|1A'\right\rangle = \sin\theta|P_x\rangle + \cos\theta|P_z\rangle, \tag{20}$$

$$\left|2A'\right\rangle = \cos\theta|P_x\rangle - \sin\theta|P_z\rangle. \tag{21}$$

The mixing angle can be computed by applying an approximate diabatization procedure to the adiabatic A' electronic wave functions obtained from a conventional *ab initio* calculation [2, 9, 11, 12].

When the H_2 polar angle α is either $\alpha = 0$ or $\alpha = \pi/2$, then symmetry considerations make the electronic states corresponding to the P_x and P_z Slater determinants good adiabatic electronic states of the Cl–H_2 system. For these geometries, the mixing angle θ must be either $\theta = 0$ or $\theta = \pi/2$. For $\theta = 0$, the P_z state is lower in energy than the P_x state, while for $\theta = \pi/2$, the P_x state is lower in energy than the P_z state. In Figure 1, we show how the Cl–H_2 interaction energy obtained in [9] for these two adiabatic states depends on the Cl–H_2 distance R, both for geometries with $\alpha = 0$ (in which the H–H bond is collinear with the Cl–H_2 distance) and for geometries with $\alpha = \pi/2$ (in which the H–H bond is perpendicular to the Cl–H_2 distance). In these plots, the H–H covalent bond length is held fixed at $r = 1.449a_0$, its $v = 0$ vibrationally averaged value.

Note that for collinear approach of the H_2 molecule, the adiabatic P_x and P_z states undergo a crossing near $R = 6.1a_0$. At that point, the mixing angle θ changes discontinuously from $\theta = \pi/2$ at large R to $\theta = 0$ at small R. We can explain this behavior using a simple picture of the Cl–H_2 interaction based on electrostatic and overlap contributions. At large R, it is more favorable for the "hole" in the Cl atom's $3p$ subshell to be oriented at right angles to the covalent bond of the incoming H_2 molecule; this leads to the most favorable quadrupole-quadrupole interaction between the H_2 molecule and the Cl atom. At small R, however, repulsive overlap interactions become more important; these are minimized if the Cl atom's hole orients itself along the axis that connects the Cl nucleus and the H_2 center of mass.

Now we investigate how the Cl–H_2 interaction changes as the H_2 molecule rotates from $\alpha = 0$ to $\alpha = \pi/2$, with both R and r held fixed. As before, we neglect SO coupling and we set r to its $v = 0$ vibrationally averaged value of $r = 1.449a_0$. Figure 2(a) shows, for the two A' adiabatic electronic states, how the Cl–H_2 interaction energy depends on α at $R = 7a_0$. In Figure 2(b) we plot, as functions of α, the contributions that the P_x and P_z diabatic states make to the

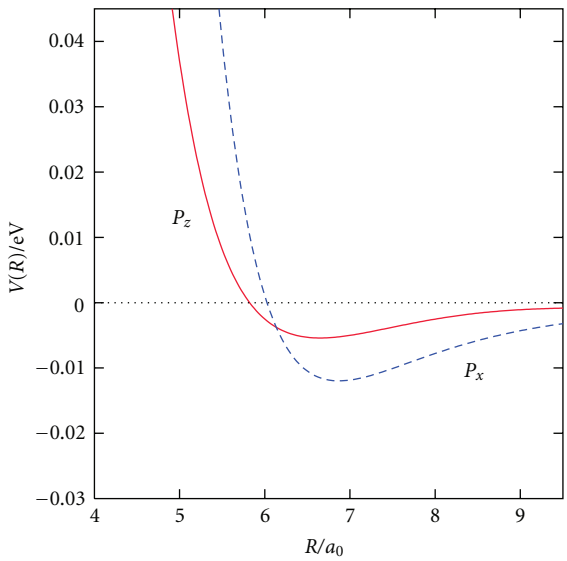

(a) Collinear $\alpha = 0$

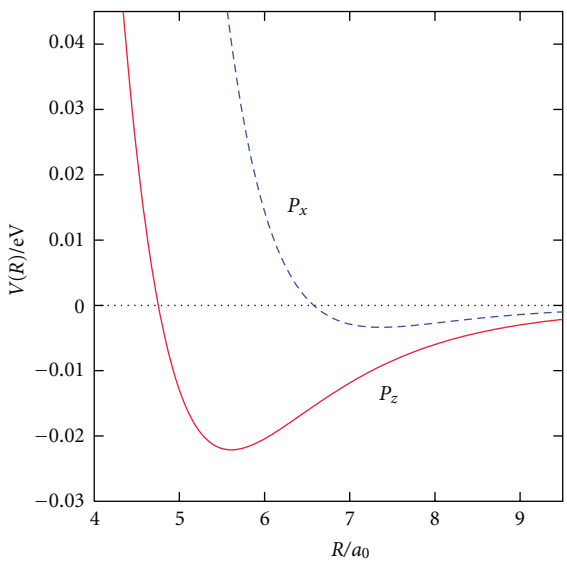

(b) T-shaped $\alpha = \pi/2$

FIGURE 1: (a) Adiabatic Cl–H_2 potential energy surfaces, as functions of the Cl–H_2 distance R, for (a) collinear and (b) T-shaped C_{2v} geometries. Solid lines indicate the potential energy for the Cl electronic configuration in which the $3p$ hole is aligned with the space-fixed z-axis; dashed lines indicate the potential energy for the Cl electronic configuration in which the $3p$ hole is aligned with the space-fixed x-axis. In both panels, r is held fixed at $r = 1.449a_0$.

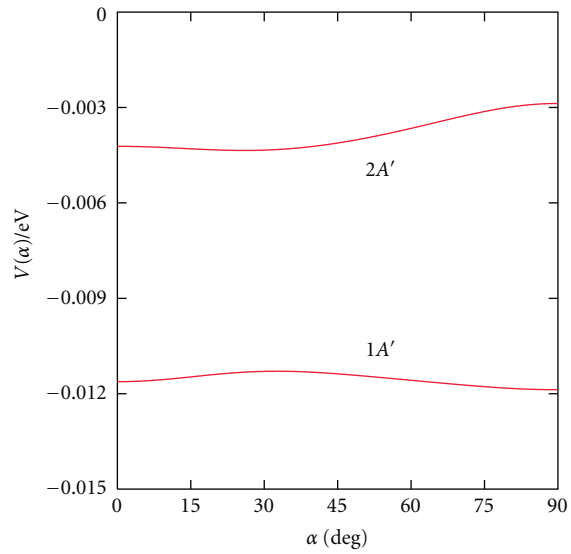

(a)

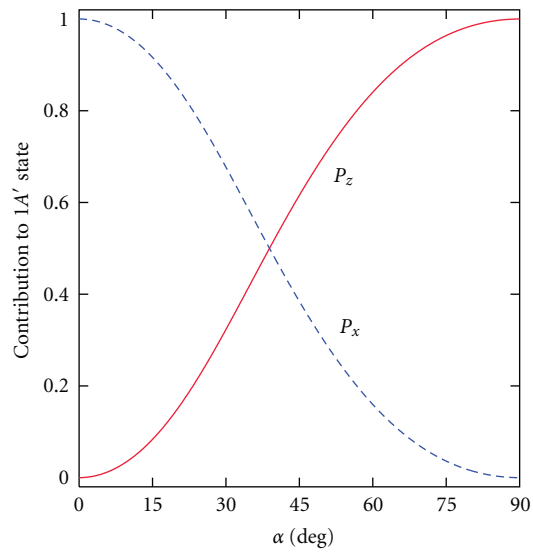

(b)

FIGURE 2: (a) Adiabatic A' potential energy surfaces for planar Cl–H_2 geometries shown as functions of the H_2 polar angle α for $R = 7a_0$ and $r = 1.449a_0$. (b) Contributions made by the Cl atom's P_x (dashed line) and P_z (solid line) Slater determinants to the lowest-energy $1A'$ electronic state shown as functions of the H_2 polar angle α for $R = 7a_0$ and $r = 1.449a_0$.

$1A'$ adiabatic state; as we see from (20), these contributions are simply $\sin^2\theta$ and $\cos^2\theta$. Figure 2(b) demonstrates that for the $1A'$ state, the hole in the Cl atom's $3p$ subshell rotates in space as α changes so that the Cl atom maintains a favorable electrostatic interaction with the H_2 quadrupole.

3.2. Electronic-Rotational Coupling in Cl–H_2 Dimers. Now we lift the restriction that $\beta = 0$ and investigate how the rotational energy levels of the H_2 molecule are perturbed by its interaction with the Cl atom. We continue to neglect SO coupling in the Cl atom.

We construct a basis set for the coupled rotational and electronic degrees of freedom of the Cl–H_2 dimer that is a direct product of functions describing the Cl atom's electronic state and functions describing the H_2 molecule's rotation. For the electronic portion of the direct product basis, we use the six Slater determinants defined in (1) through (6); this will simplify the subsequent incorporation of SO coupling. For the rotational portion of the direct

product basis, we use the spherical harmonics $Y_{j,m_j}(\alpha,\beta)$ with even values of the H_2 rotational quantum number j.

In this work, we limit the possible j values to $j = 0$ and $j = 2$; this leads to a basis set with 36 orthonormal direct product electronic-rotational basis functions. In the absence of SO coupling, however, the 36×36 Hamiltonian matrix splits into two uncoupled 18×18 blocks that are, respectively, associated with the spin-up and spin-down Slater determinants. The two 18×18 blocks have a common set of eigenvalues.

We could exploit the cylindrical symmetry of the Cl–H_2 system to further factorize the Hamiltonian matrix. This would involve rewriting the electronic portion of the basis set in terms of complex linear combinations of P_x and P_y that are eigenfunctions of the $\hat{L}_z$ operator, with eigenvalues $\hbar\lambda_z$:

$$\frac{\left(P_x + iP_y\right)}{\sqrt{2}} \longrightarrow \lambda_z = +1, \tag{22}$$

$$\frac{\left(P_x - iP_y\right)}{\sqrt{2}} \longrightarrow \lambda_z = -1. \tag{23}$$

Because of the system's cylindrical symmetry, the quantum number $\Lambda = \lambda_z + m_j$, which, after multiplication by $\hbar$, is the z-axis projection of the sum of the electronic orbital angular momentum and the H_2 rotational angular momentum, is rigorously good in the absence of SO coupling. If we were to express the SO-free Hamiltonian matrix in terms of the complex basis functions of (22) and (23), the two 18×18 blocks of the matrix would therefore factor into uncoupled subblocks corresponding to the allowed values of Λ. Although we do not employ this approach here, we will use Λ to classify the overall symmetry of the SO-free Cl–H_2 wave functions. For the basis set employed here, Λ ranges from -3 to $+3$ in steps of one. In analogy with the nomenclature for diatomic molecules, we will denote Cl–H_2 wave functions with $|\Lambda| = 0, 1, 2$, or 3 as σ, π, δ, or ϕ states, respectively.

For a fixed value of the Cl–H_2 distance R, the elements of the 36×36 electronic-rotational Hamiltonian matrix can be written as

$$\left\langle P_q Y_{j,m_j} \middle| \hat{V}(\alpha,\beta;R) + \left(\frac{B}{\hbar^2}\right)\hat{J}^2 \middle| P_{q'} Y_{j',m'_j} \right\rangle, \tag{24}$$

where q and q' represent space-fixed Cartesian directions, B is the H_2 rotational constant (here taken to have the value $59.06\,\mathrm{cm}^{-1}$), and $\hat{V}(\alpha,\beta;R)$ describes the Cl–H_2 interaction. The analogous matrix element in which the electronic portions of the basis functions are represented by $\overline{P}_q$ and $\overline{P}_{q'}$ has the same value as the matrix element in (24). Matrix elements that involve a spin-up and a spin-down Slater determinant are zero in the absence of SO coupling.

Because the Slater determinants P_q and $P_{q'}$ are orthogonal unless $q = q'$, the kinetic energy portion of (24) can be evaluated quite easily; it is given by

$$Bj(j+1)\delta_{q,q'}\delta_{j,j'}\delta_{m_j,m'_j}. \tag{25}$$

After writing out explicitly the integration over the H_2 angles α and β, the potential energy portion of (24) becomes

$$\int_{-1}^{1} d(\cos\alpha) \int_0^{2\pi} d\beta Y^*_{j,m_j}(\alpha,\beta) F_{q,q'}(\alpha,\beta;R) Y_{j',m'_j}(\alpha,\beta), \tag{26}$$

where

$$F_{q,q'}(\alpha,\beta;R) = \left\langle P_q \middle| \hat{V}(\alpha,\beta;R) \middle| P_{q'} \right\rangle. \tag{27}$$

Here, we compute the integrals in (26) by numerical quadrature, using the 240-point spherical t-design specified in [13].

To evaluate $F_{q,q'}(\alpha,\beta;R)$, we introduce a rotated system of Cartesian axes, which we denote (u,v,z). The u and v axes rotate in the space-fixed (x,y) plane as the H_2 azimuthal angle β changes, so that the H_2 molecule always resides in the (u,z) plane. The Slater determinants P_x and P_y, defined in the space-fixed coordinate system, are related to their analogues P_u and P_v, defined in the rotated coordinate system, through

$$P_x = P_u \cos\beta - P_v \sin\beta, \tag{28}$$

$$P_y = P_u \sin\beta + P_v \cos\beta. \tag{29}$$

Equipped with this relationship, we can now evaluate $F_{q,q'}(\alpha,\beta;R)$, where q and q' are directions in the space-fixed coordinate system, in terms of integrals over P_u, P_v, and P_z. Doing this, we obtain

$$F_{x,x}(\alpha,\beta;R) = \cos^2\beta\left\langle P_u \middle| \hat{V} \middle| P_u \right\rangle + \sin^2\beta\left\langle P_v \middle| \hat{V} \middle| P_v \right\rangle, \tag{30}$$

$$F_{y,y}(\alpha,\beta;R) = \sin^2\beta\left\langle P_u \middle| \hat{V} \middle| P_u \right\rangle + \cos^2\beta\left\langle P_v \middle| \hat{V} \middle| P_v \right\rangle, \tag{31}$$

$$F_{x,y}(\alpha,\beta;R) = \sin\beta\cos\beta\left(\left\langle P_u \middle| \hat{V} \middle| P_u \right\rangle - \left\langle P_v \middle| \hat{V} \middle| P_v \right\rangle\right), \tag{32}$$

$$F_{x,z}(\alpha,\beta;R) = \cos\beta\left\langle P_u \middle| \hat{V} \middle| P_z \right\rangle, \tag{33}$$

$$F_{y,z}(\alpha,\beta;R) = \sin\beta\left\langle P_u \middle| \hat{V} \middle| P_z \right\rangle, \tag{34}$$

where, for the sake of brevity, we have suppressed the $(\alpha,\beta;R)$ dependence of $\hat{V}$. Note that $\langle P_u|\hat{V}|P_v\rangle$ and $\langle P_v|\hat{V}|P_z\rangle$ are both zero by reasons of symmetry.

The quantities $\langle P_u|\hat{V}|P_u\rangle$, $\langle P_v|\hat{V}|P_v\rangle$, and $\langle P_u|\hat{V}|P_z\rangle$ are the same as those in (2) through (4) of [9]. They depend on α and R but are independent of β. As a consequence, Cl–H_2 electronic-rotational basis functions with different values of m_j are coupled only by the trigonometric functions of β that are shown explicitly in (30) through (34). $F_{x,x}$ and $F_{y,y}$ couple H_2 rotational states with $|m_j - m'_j| = 0$ or 2, $F_{x,y}$ couples H_2 rotational states with $|m_j - m'_j| = 2$, and $F_{x,z}$ and $F_{y,z}$ couple H_2 rotational states with $|m_j - m'_j| = 1$. $F_{z,z}$ has no dependence on β and therefore does not couple basis functions with different m_j values.

Constructing and diagonalizing the 36×36 electronic-rotational Hamiltonian matrix at a series of R values gives

the Cl–H_2 curves shown in Figure 3, which we now discuss in some detail. The curves fall into three distinct groups, labeled as A, B, and C. The two curves in group A correlate smoothly with the $j = 0$ rotational level of the H_2 molecule as $R \to \infty$, while those in groups B and C correlate with $j = 2$ states of the H_2 molecule in this limit. All of the B curves, at large R, correlate with electronic-rotational basis functions that involve the Cl atom's P_z Slater determinant. The C curves, on the other hand, correlate at large R with electronic-rotational basis functions involving the P_x and P_y Slater determinants of the Cl atom.

We begin by considering the two curves (one σ and one π) in group A. Both curves are attractive at long range, but the minimum of the σ curve is deeper and occurs at a smaller R value. The minimum for the σ curve occurs at $R_{\min} = 5.85a_0$, where $E = -15.9$ meV. The minimum for the π curve is at $R_{\min} = 7.08a_0$, where $E = -6.5$ meV. The σ curve correlates at large R with the P_z Slater determinant of the Cl atom's $3p$ subshell; for this Slater determinant, the $3p$ hole of the Cl atom is oriented along the space-fixed z axis, which is the direction of approach of the incoming H_2 molecule. The π curve, by contrast, correlates at large R values with the P_x and P_y Slater determinants, for which the Cl atom's $3p$ hole is oriented in the (x, y) plane. The σ curve thus minimizes short-range repulsive overlap interactions between Cl and H_2 and permits closer approach of the incoming H_2 molecule.

Group B includes three curves: one σ, one π, and one δ. These curves all correlate smoothly with the P_z Slater determinant as $R \to \infty$, so the Cl atom's $3p$ hole is aligned with the space-fixed z axis for large R. For the δ curve, the H_2 rotational state at large R corresponds to the ($j = 2$, $m_j = \pm 2$) spherical harmonic. In this state, the H_2 molecule can be viewed classically as rotating in the (x, y) plane. This orientation of the rotating H_2 molecule both maximizes its attractive electrostatic quadrupole-quadrupole interaction with the Cl atom and minimizes short-range Cl–H_2 repulsive interactions at small R values. Consequently, of the three group B curves, the δ curve has the deepest minimum.

The π curve from group B correlates at large R with electronic-rotational basis functions that are direct products of the H_2 ($j = 2$, $m_j = \pm 1$) spherical harmonics and the Cl atom's P_z Slater determinant. As $R \to \infty$, therefore, the π character of this curve is associated with the rotational motion of the H_2 molecule. Figure 3 shows, however, that this curve undergoes an avoided crossing with the group A π curve near $R = 5.5a_0$.

To understand the nature of this avoided crossing in more detail, we project the wave function for the group A π curve onto two pairs of electronic-rotational direct product basis functions: (1) the two functions $|P_x\ Y_{0,0}\rangle$ and $|P_y\ Y_{0,0}\rangle$ and (2) the two functions $|P_z\ Y_{2,1}\rangle$ and $|P_z\ Y_{2,-1}\rangle$. The first pair of functions describes the group A π curve at large R values, while the second pair of functions describes the group B π curve at large R values. Figure 4 shows the R dependence of the contributions that these two pairs of basis functions make to the π curve of group A.

It is clear that, for the entire range of R values shown in Figure 4, the makeup of the group A π curve is dominated by these two pairs of basis functions; summed together, their

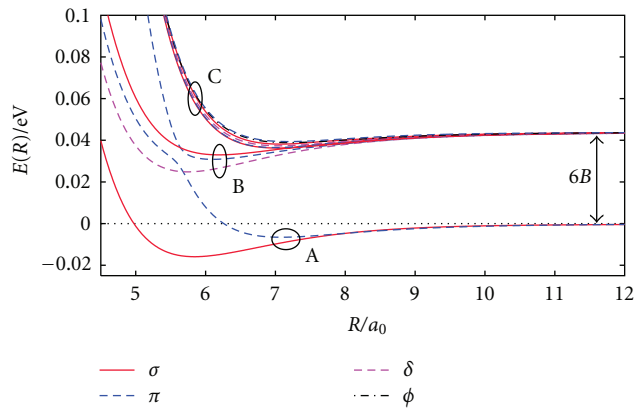

Figure 3: Coupled electronic-rotational Cl–H_2 energy curves that correlate with the $j = 0$ and $j = 2$ states of H_2 shown as functions of the Cl–H_2 distance R. Spin-orbit effects are neglected, and the H_2 bond length is held fixed at $r = 1.449a_0$.

contributions represent over 99% of the curve's character. At large R values, the curve can be described entirely by the $|P_x\ Y_{0,0}\rangle$ and $|P_y\ Y_{0,0}\rangle$ direct product functions, demonstrating that the π character of the state arises from the Cl atom's $3p$ subshell. At small R values, however, the curve is described entirely by the $|P_z\ Y_{2,1}\rangle$ and $|P_z\ Y_{2,-1}\rangle$ direct product functions; here, the π character of the state arises from the rotational motion of the H_2 molecule. The crossover in the description of the π curve of group A reflects a strong interaction between these two zero-order states, an interaction that arises from the $F_{x,z}$ and $F_{y,z}$ functions of (33) and (34). The result is to strongly couple the electronic and rotational degrees of freedom of the Cl–H_2 dimer near $R = 5.5a_0$.

We have also taken the group A σ curve and projected it onto the direct product basis function $|P_z\ Y_{0,0}\rangle$ to assess the contribution that this zero-order state makes to the curve. Figure 4 indicates that this zero-order state provides a very good description of the group A σ curve, accounting for more than 90% of its character over the entire range of R values shown there. This demonstrates that the group A σ curve can be closely approximated by the interaction between a pure $j = 0$ *para*-H_2 molecule and a Cl atom described by the P_z Slater determinant.

4. Cl–H_2 Including Spin-Orbit Coupling

Now we ask how the results summarized in Figures 3 and 4 change when we include the effects of SO coupling. To do this, we simply add the appropriate matrix elements of the SO operator (see (8)) to the 36×36 Hamiltonian matrix expressed in the direct product basis set, and then compute the eigenvalues of the new matrix at a series of R values. The calculations of [9] indicate that, in the Cl–H_2 van der Waals region, the triatomic system's SO matrix elements are nearly independent of the Cl–H_2 geometry and have values nearly identical to those for an isolated Cl atom. This justifies the approximation implicit in our calculations, namely that the

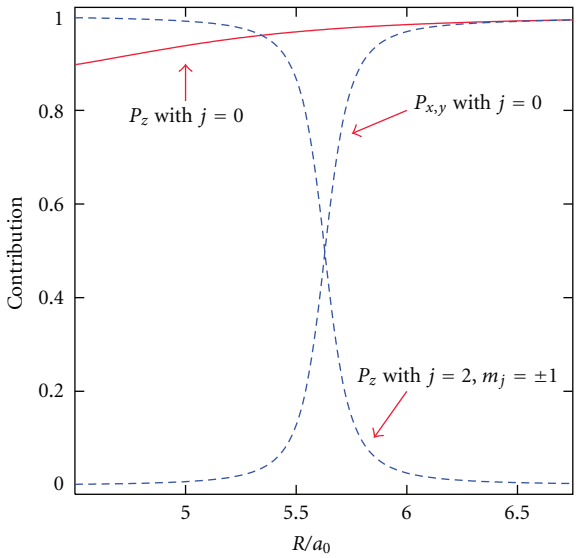

Figure 4: Solid line: the contribution made by the $|P_z\ Y_{0,0}\rangle$ basis function to the lowest σ Cl–H_2 $E(R)$ curve shown in Figure 3. Dashed lines: contributions made by the $|P_{x,y}\ Y_{0,0}\rangle$ pair of basis functions and the $|P_z\ Y_{2,\pm 1}\rangle$ pair of basis functions to the lowest π Cl–H_2 $E(R)$ curve shown in Figure 3.

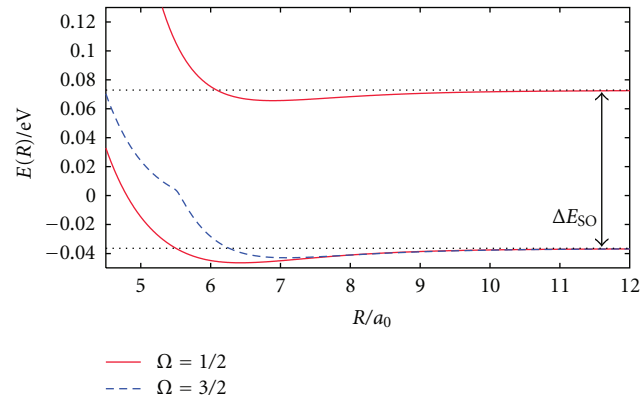

Figure 5: Coupled electronic-rotational Cl–H_2 energy curves that correlate with the $j = 0$ rotational state of H_2 shown as functions of the Cl–H_2 distance R. Spin-orbit effects are included; the horizontal dashed lines indicate the asymptotic energies of the Cl–H_2 dimer as $R \to \infty$ for the lower and upper spin-orbit levels of the Cl atom.

Table 1: Combinations (j_z, m_j) of azimuthal angular momentum quantum numbers that can couple together to produce a given positive Ω value.

$\Omega = 1/2$	$\Omega = 3/2$	$\Omega = 5/2$	$\Omega = 7/2$
$(+3/2, -1)$	$(+3/2, 0)$	$(+3/2, +1)$	$(+3/2, +2)$
$(+1/2, 0)$	$(+1/2, +1)$	$(+1/2, +2)$	
$(-1/2, +1)$	$(-1/2, +2)$		
$(-3/2, +2)$			

V_{SO} matrix for the free Cl atom is a good approximation of the effects of SO coupling in the Cl–H_2 dimer. For a given value of R, and in the absence of accidental degeneracies, the new Hamiltonian matrix has 18 distinct doubly degenerate eigenvalues. Kramers [14] explained that a system with a single unpaired electron would always, in the absence of an external magnetic field, have doubly degenerate energy levels; the two states that make up a single doubly degenerate energy level are sometimes called a Kramers pair.

As before, the system's cylindrical symmetry introduces a rigorously good quantum number that, when multiplied by $\hbar$, gives the z-axis projection of the system's total (electronic spin plus electronic orbital plus H_2 rotational) angular momentum. Here we call this quantum number Ω; its value is given by $\Omega = j_z + m_j$, and for the basis set employed here, the possible values of Ω range from $-7/2$ to $7/2$ in steps of one. Although we have not exploited the system's cylindrical symmetry to block-diagonalize the Hamiltonian matrix, we use Ω to classify the symmetry of the Cl–H_2 wave functions and to gain some physical insight into the shapes of the system's energy curves $E(R)$.

In Table 1, we list the combinations of the j_z and m_j quantum numbers that can generate each of the four positive allowed Ω values. The corresponding negative Ω values can be obtained by reversing the sign of both j_z and m_j. In the following discussion, we consider only the states that have positive Ω values, as the states with negative Ω values have identical energies. We will refer to this table and to the charge densities of the two SO levels of an isolated Cl atom ((17) through (19)), as we discuss the role that SO coupling has on the Cl–H_2 energy curves.

As Table 1 indicates, the $j = 0$ state of the H_2 molecule, which has $m_j = 0$ as well, can either (1) form a Cl–H_2 state with $\Omega = 3/2$ by combining with the $\psi_{g,+3/2}$ state of the Cl atom or (2) form a Cl–H_2 state with $\Omega = 1/2$ by combining with the $\psi_{g,+1/2}$ state or the $\psi_{e,+1/2}$ state of the Cl atom. Consequently, there are three distinct Cl–H_2 curves that correlate as $R \to \infty$ with the $j = 0$ ground rotational state of the H_2 molecule. Two of the three curves are associated with the Cl atom's lower SO energy level, and one is associated with the atom's upper SO energy level. These curves, shown in Figure 5, are the most important ones for understanding the interaction between Cl and an approaching *para*-H_2 molecule.

All three curves exhibit relatively shallow van der Waals minima. The $\Omega = 1/2$ state that correlates with the Cl atom's lower SO energy level has the deepest minimum, which occurs at $R = 6.46a_0$. At this R value, the depth of the Cl–H_2 curve, measured with respect to the $R = \infty$ asymptote, is 10.0 meV. The other two states have shallower minima, which occur at larger R values: the minimum for the $\Omega = 1/2$ state that correlates with the upper SO energy level is at $R = 6.89a_0$, while that for the $\Omega = 3/2$ state is at $R = 7.09a_0$. The depths of these minima, measured with respect to the $R = \infty$ asymptotes, are, respectively, 7.3 meV and 6.5 meV. The relative locations and depths of the three minima can

be understood by examining the charge densities of the Cl electronic states that are associated with each curve.

For the $\Omega = 1/2$ curve that correlates with the lower SO energy level, the Cl atom is described at large R by the $\psi_{g,+1/2}$ electronic wave function. This Cl atomic state has a depletion of electron density along the z axis (see (18)), which is the direction of approach of the incoming H_2 molecule. Consequently, of the three curves shown in Figure 5, this curve allows the H_2 molecule to approach the Cl atom most closely. For the $\Omega = 3/2$ curve, on the other hand, the Cl atom is described at large R by the $\psi_{g,+3/2}$ electronic wave function; as (17) shows, the electron density for this state of the Cl atom is depleted in the (x, y) plane and built up along the z axis. Of the three curves shown in Figure 5, this curve has its minimum at the largest R value. Finally, for the $\Omega = 1/2$ curve that correlates with the upper SO energy level, the Cl atom's large-R character is that of the $\psi_{e,+1/2}$ state. In this state, the atom's $3p$ "hole" is completely orientationally delocalized (see (19)). This leads to a minimum that occurs at an R value between the minima for the two other curves.

We now ask, for the two $\Omega = 1/2$ curves depicted in Figure 5, how the approach of the incoming H_2 molecule distorts the electronic structure of the Cl atom. To answer this question, we take the Cl–H_2 wave functions for the two curves and project them onto either the $\psi_{g,+1/2}$ (for the lower curve) or the $\psi_{e,+1/2}$ (for the upper curve) Cl atomic wave function. In computing these projections, we sum over all of the H_2 fragment's rotational states. Figure 6(a) shows, as a function of the Cl–H_2 distance R, the fractional contributions that these two pure atomic SO states make to the corresponding Cl–H_2 dimer wave functions. For large R, the Cl electronic structure is essentially unperturbed by the H_2 molecule. As R decreases below about $6a_0$, however, the impinging H_2 molecule begins to mix some excited SO character into the wave function of the lower curve, and some ground SO character into the wave function of the upper curve.

For these two $\Omega = 1/2$ curves, Cl–H_2 interactions also perturb the rotational degrees of freedom of the H_2 fragment at small R values. This leads to a mixing of some $j = 2$ character into the H_2 molecule's rotational wave function. To measure this perturbation, we project the two Cl–H_2 $\Omega = 1/2$ wave functions onto the $j = 0$ H_2 molecular rotational wave function. In computing these projections, we sum over all of the Cl fragment's SO states. Figure 6(b) shows how the contribution that the H_2 $j = 0$ state makes to the overall dimer wave function changes with R. For the range of R values shown here, the character of both $\Omega = 1/2$ curves is dominated by the $j = 0$ H_2 rotational state.

Figures 7 through 9 complete our survey of the Cl–H_2 energy curves associated with the lower SO energy level. In these figures, the curves whose large-R asymptotic values are roughly 7 meV all correlate, as $R \to \infty$, with the H_2 molecule's $j = 2$ rotational energy level. For the $\Omega = 1/2$, 5/2, and 7/2 states (Figures 7 and 9), these curves fall into two groups distinguished mainly by the position of their short-range repulsive walls. The curves whose repulsive walls occur at smaller R values are associated with the Cl atom's $\psi_{g,\pm 1/2}$ states, which have a depletion of electron density along the z axis. The curves whose repulsive walls occur at larger R values are associated with the Cl atom's $\psi_{g,\pm 3/2}$ states, which do not exhibit depleted electron density along the z axis.

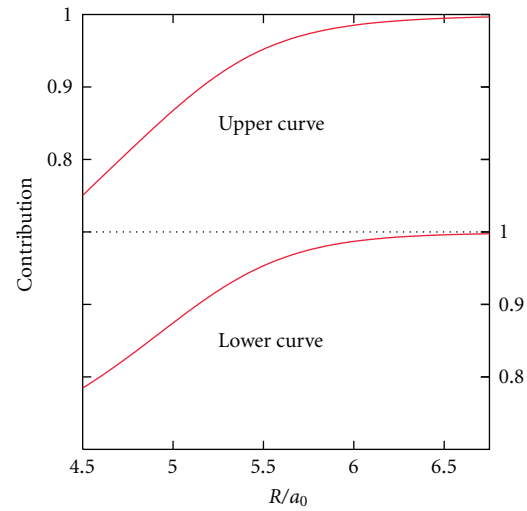

(a)

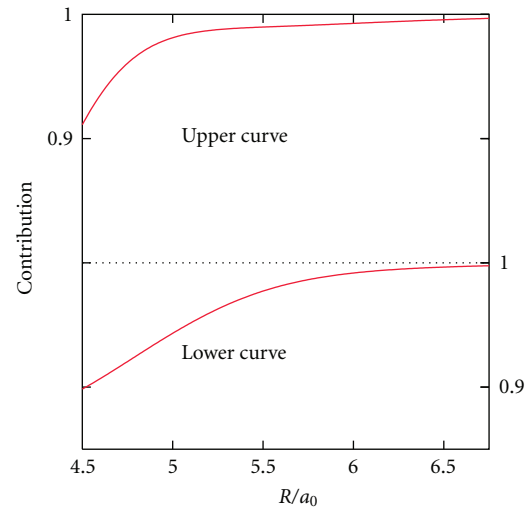

(b)

Figure 6: (a) The contribution made by the Cl atom's respective $\psi_{g,+1/2}$ or $\psi_{e,+1/2}$ spin-orbit electronic state to the two $\Omega = 1/2$ curves shown in Figure 5. (b) The contribution made by the H_2 $j = 0$ rotational state to the Cl–H_2 wave function for the two $\Omega = 1/2$ curves shown in Figure 5.

The $\Omega = 3/2$ curves depicted in Figure 8 exhibit more complicated behavior. The uppermost curve shown there is associated with the Cl atom's $\psi_{g,+3/2}$ state, and thus its repulsive wall begins to manifest itself at larger R values. The other three curves, however, participate in a pair of avoided crossings near $R = 5.5a_0$, close to where the avoided crossing observed in Figure 3 occurred. The unusual "kink" seen in Figure 5 is associated with this pair of avoided crossings.

Figure 10 shows this pair of avoided crossings at higher magnification. The three curves, in order of increasing energy, correlate in the large R limit with (1) the $\psi_{g,+3/2}$ Cl

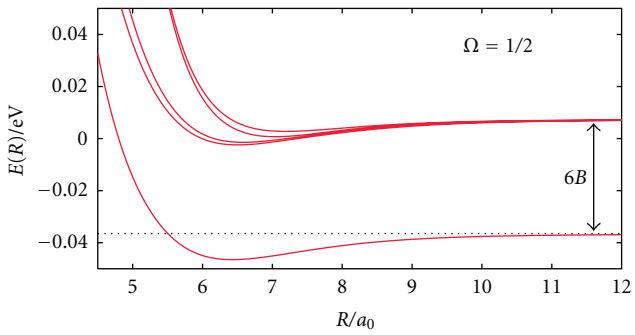

Figure 7: All of the Cl–H_2 dimer's $\Omega = 1/2$ coupled electronic-rotational states that correlate with the lower spin-orbit level of the Cl atom are shown as functions of the Cl–H_2 distance R. The horizontal dashed line indicates the dimer's asymptotic energy, as $R \to \infty$, for the lower spin-orbit level of the Cl atom and the $j = 0$ state of H_2.

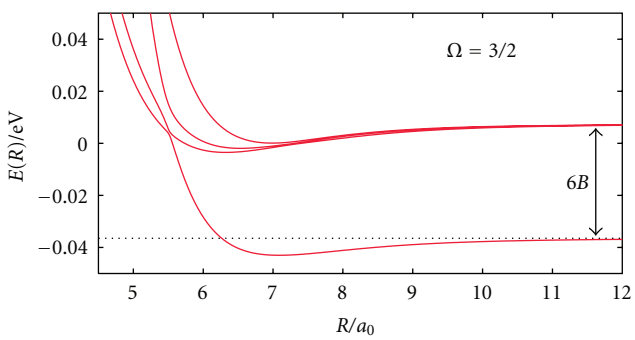

Figure 8: All of the Cl–H_2 dimer's $\Omega = 3/2$ coupled electronic-rotational states that correlate with the lower spin-orbit level of the Cl atom are shown as functions of the Cl–H_2 distance R. The horizontal dashed line indicates the dimer's asymptotic energy, as $R \to \infty$, for the lower spin-orbit level of the Cl atom and the $j = 0$ state of H_2.

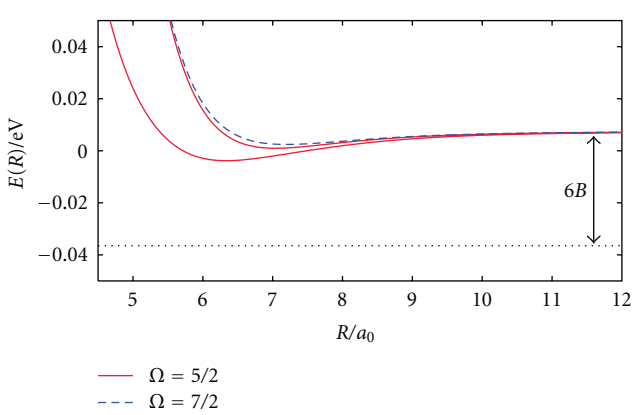

Figure 9: All of the Cl–H_2 dimer's $\Omega = 5/2$ and $\Omega = 7/2$ coupled electronic-rotational states that correlate with the lower spin-orbit level of the Cl atom are shown as functions of the Cl–H_2 distance R. The horizontal dashed line indicates the dimer's asymptotic energy, as $R \to \infty$, for the lower spin-orbit level of the Cl atom and the $j = 0$ state of H_2.

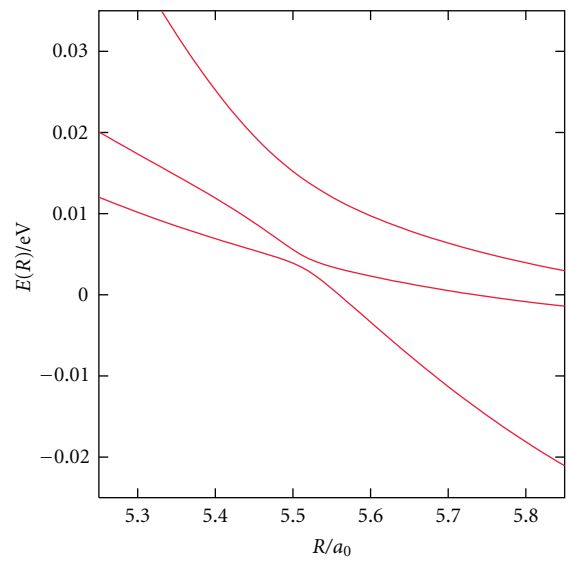

Figure 10: A magnified view of three $\Omega = 3/2$ curves shown in Figure 8. This figure shows the pair of avoided crossings near $R = 5.5a_0$ that affect the $\Omega = 3/2$ coupled electronic-rotational states that correlate with the lower Cl spin-orbit level.

atomic state coupled with the $(j = 0, m_j = 0)$ rotational state of H_2; (2) the $\psi_{g,-1/2}$ Cl atomic state coupled with the $(j = 2, m_j = 2)$ rotational state of H_2; and (3) the $\psi_{g,+1/2}$ Cl atomic state coupled with the $(j = 2, m_j = 1)$ rotational state of H_2. The pair of avoided crossings shown in Figure 10 is analogous to the avoided crossing between the group A and group B π curves shown in Figure 3. The additional complexity observed in Figure 10 arises from the fact that, as Table 1 shows, three different values of the H_2 molecule's m_j quantum number can combine with an appropriate SO level of the Cl atom to form a dimer state with $\Omega = 3/2$. Although the avoided crossings shown in Figure 10, like that shown in Figure 3, demonstrate that there are regions of configuration space where the Cl–H_2 dimer exhibits strong electronic-rotational coupling, these regions of configuration space are at moderately high energies on the repulsive wall of the dimer's potential energy surface.

Finally, in Figure 11, we show all of the curves that correlate at large R with the Cl atom's upper SO level. Only one of these curves, with $\Omega = 1/2$, correlates with the $j = 0$ state of the H_2 molecule; the others correlate with the H_2 molecule's $j = 2$ excited rotational state. All six curves shown in this figure have very similar shapes; this is because the upper SO level of the Cl atom, with its orientationally delocalized $3p$ hole, appears isotropic to the incoming H_2 molecule.

We close by computing the Cl–H_2 interaction curves $E(R)$, including the effects of SO coupling, under the assumption that the H_2 molecule retains pure $j = 0$ character at all values of R. We do this simply by removing all of the direct product basis functions with $j > 0$ from the basis set used to express the Cl–H_2 dimer wave function; this leads to a 6×6 matrix representation of the Cl–H_2 Hamiltonian that has three doubly degenerate eigenvalues,

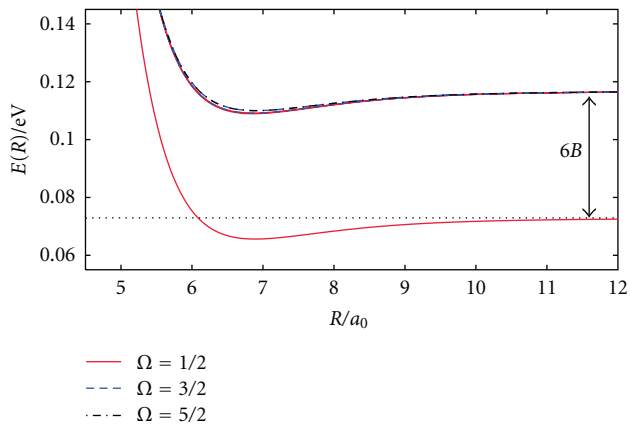

Figure 11: All of the Cl–H_2 dimer's coupled electronic-rotational states that correlate with the upper spin-orbit level of the Cl atom are shown as functions of the Cl–H_2 distance R. The horizontal dashed line indicates the dimer's asymptotic energy, as $R \to \infty$, for the upper spin-orbit level of the Cl atom and the $j = 0$ state of H_2.

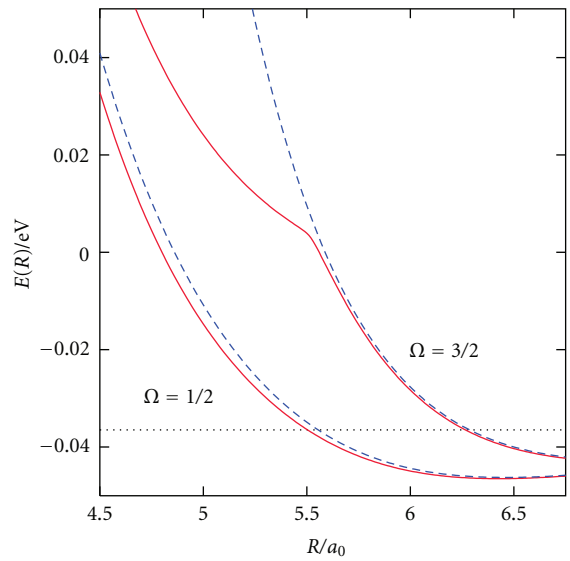

(a)

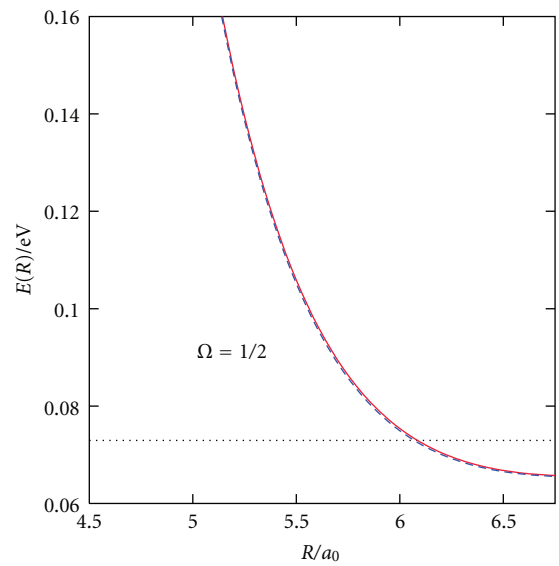

(b)

Figure 12: A comparison of the three Cl–H_2 curves that correlate with $j = 0$ H_2 molecules when the H_2 molecule is either frozen in its $j = 0$ state (dashed lines) or allowed to mix some $j = 2$ character into its rotational wave function (solid lines). (a) shows, as functions of the Cl–H_2 distance R, curves for the two states that correlate with the lower spin-orbit state of the Cl atom; (b) shows curves for the state that correlates with the upper spin-orbit state of the Cl atom. The horizontal dashed lines show the respective asymptotic dimer energies as $R \to \infty$. The two curves shown in (b) are nearly indistinguishable from one another.

or three Kramers pairs. These three eigenvalues represent the interaction curves $E(R)$ obtained using the pure $j = 0$ approximation for the H_2 fragment. In Figure 12, we show these three curves and compare them with the analogous curves computed using the larger 36×36 Hamiltonian matrix that includes $j = 2$ states of the H_2 fragment. The three curves obtained from the larger Hamiltonian matrix were first shown in Figure 5.

We see from Figure 12 that the depths and positions of the van der Waals minima for these three curves change very little when we impose the pure $j = 0$ approximation for the H fragment. For example, the depth of the $\Omega = 1/2$ curve that correlates with the Cl atom's lower SO state (shown in Figure 12(a)) changes by about 0.5% when we impose this approximation. This is in sharp contrast to the case for the B-H_2 and Al-H_2 dimers [7], for which the zero-point-corrected binding energies change by 15% and 22%, respectively, when the H_2 fragment is frozen in its $j = 0$ state. It appears that the anisotropy of the underlying diabatic potential energy surfaces is substantially larger for the B-H_2 and Al-H_2 systems than for the Cl–H_2 system; this leads to a greater perturbation of the H_2 molecule's rotational wave function in the region of the van der Waals minima of the B-H_2 and Al-H_2 systems.

For the two $\Omega = 1/2$ curves shown in Figure 12, we see that the pure $j = 0$ approximation reproduces the actual Cl–H_2 interaction curves very well; the main difference seems to be that the $\Omega = 1/2$ curve that correlates with the lower SO level of the Cl atom has a slightly stiffer repulsive wall if the H_2 molecule is held fixed in its $j = 0$ rotational state. For the $\Omega = 3/2$ curve that correlates with the lower SO level of the Cl atom, the pure $j = 0$ approximation is of course completely incapable of reproducing the true Cl–H_2 interaction for R values below $R = 5.5a_0$; this is the region of configuration space where strong electronic-rotational coupling leads to the avoided crossings shown in Figure 10, and the $j = 0$ approximation is simply inapplicable there. However, this region of configuration space is relatively high on the repulsive wall of the $\Omega = 3/2$ curve; because the experimental studies of Cl-doped solid *para*-H_2 are carried out at $T \approx 2$ K, it is unlikely that the Cl atom's H_2 neighbors spend a significant portion of time exploring this portion of the $\Omega = 3/2$ potential energy curve.

5. Summary

We have computed a series of one-dimensional energy curves $E(R)$ for the Cl–*para*-H_2 dimer by diagonalizing the dimer's combined electronic-rotational Hamiltonian matrix. We express the Hamiltonian matrix in terms of a direct product basis set that facilitates the inclusion of SO coupling effects. The gross features of the dimer's $E(R)$ curves, such as the depths and positions of the curves' van der Waals minima, can be rationalized by considering the charge densities associated with the lower and upper SO levels of the Cl atom.

We find that electronic-rotational coupling in the Cl–H_2 dimer is strong for Cl–H_2 distances near $R = 5.5a_0$. In the system where SO effects are ignored, this coupling gives rise to an avoided crossing between two Cl–H_2 states with π symmetry: one that correlates at large R with the $j = 0$ H_2 rotational level and one that correlates with the $j = 2$ rotational level. Once SO effects are included, this avoided crossing becomes a pair of avoided crossings associated with three of the Cl–H_2 dimer's $\Omega = 3/2$ states: one of which correlates at large R with the $j = 0$ H_2 rotational level and two of which correlate with the $j = 2$ rotational level.

By removing $j = 2$ H_2 rotational states from the direct product basis set used to express the Cl–H_2 Hamiltonian, we can assess how the assumption that the *para*-H_2 fragment retains its pure $j = 0$ identity might affect the shape of the Cl–*para*-H_2 energy curves. We find that the positions and depths of the system's van der Waals minima are virtually unaffected when the H_2 fragment is restricted to its pure $j = 0$ rotational state. This suggests that the H_2 molecules in Cl-doped solid *para*-H_2 can probably be treated as pure $j = 0$ objects without a significant loss of accuracy.

Acknowledgments

R. J. Hinde thanks D. T. Anderson and K. R. Brown for helpful discussions. This work was supported by the US National Science Foundation through Grant CHE-0848841.

References

[1] P. L. Raston and D. T. Anderson, "The spin-orbit transition of atomic chlorine in solid H_2, HD, and D_2," *Journal of Chemical Physics*, vol. 126, no. 2, Article ID 021106, 4 pages, 2007.

[2] J. Klos, M. M. Szczesniak, and G. Chalasinski, "Paradigm prereactive van der Waals complexes: X–HX and X–H_2 (X = F, Cl, Br)," *International Reviews in Physical Chemistry*, vol. 23, no. 4, pp. 541–571, 2004.

[3] X. Wang, W. Dong, C. Xiao et al., "The extent of non-Born-Oppenheimer coupling in the reaction of Cl(^{2}P) with *para*-H_2," *Science*, vol. 322, no. 5901, pp. 573–576, 2008.

[4] D. Skouteris, D. E. Manolopoulos, W. Bian, H. J. Werner, L. H. Lai, and K. Liu, "Van der Waals interactions in the Cl + HD reaction," *Science*, vol. 286, no. 5445, pp. 1713–1716, 1999.

[5] J. R. Krumrine, S. Jang, M. H. Alexander, and G. A. Voth, "Quantum molecular dynamics and spectral simulation of a boron impurity in solid *para*-hydrogen," *Journal of Chemical Physics*, vol. 113, no. 20, pp. 9079–9089, 2000.

[6] Q. Wang, M. H. Alexander, and J. R. Krumrine, "An ab initio based model for the simulation of multiple ^{2}P atoms embedded in a cluster of spherical ligands, with application to Al in solid *para*-hydrogen," *Journal of Chemical Physics*, vol. 117, no. 11, pp. 5311–5318, 2002.

[7] J. Williams and M. H. Alexander, "Potential energy surfaces for and energetics of the weakly-bound Al–H_2 and B–H_2 complexes," *Journal of Chemical Physics*, vol. 112, no. 13, pp. 5722–5730, 2000.

[8] T. Zeng, H. Li, R. J. Le Roy, and P. N. Roy, "'Adiabatic hindered rotor' treatment of the *para*-hydrogen-water complex," *Journal of Chemical Physics*, vol. 135, no. 9, Article ID 094304, 15 pages, 2011.

[9] G. Capecchi and H. J. Werner, "Ab initio calculations of coupled potential energy surfaces for the Cl($^2P_{3/2}$,$^2P_{1/2}$) + H_2 reaction," *Physical Chemistry Chemical Physics*, vol. 6, no. 21, pp. 4975–4983, 2004.

[10] M. Dagenais, J. W. C. Johns, and A. R. W. McKellar, "Precision measurement measurement of the ground state ($^2P_{1/2}$ $-^2P_{3/2}$) splitting of atomic chlorine by CO_2 laser Zeeman spectroscopy," *Canadian Journal of Physics*, vol. 54, no. 14, pp. 1438–1441, 1976.

[11] J. Kłos, G. Chałasiński, and M. M. Szczęśniak, "Modeling of adiabatic and diabatic potential energy surfaces of Cl(^{2}P)$\cdots$ H_2($^1\sum_g^+$) prereactive complex from ab initio calculations," *Journal of Chemical Physics*, vol. 117, no. 10, pp. 4709–4719, 2002.

[12] Y. Kurosaki and T. Takayanagi, "Global *ab initio* potential energy surfaces for the lowest three doublet states ($1^2\,A'$, $2^2\,A'$, and $1^2\,A''$) of the BrH_2 system," *Journal of Chemical Physics*, vol. 119, no. 15, pp. 7838–7856, 2003.

[13] R. H. Hardin and N. J. A. Sloane, "McLaren's improved snub cube and other new spherical designs in three dimensions," *Discrete and Computational Geometry*, vol. 15, no. 4, pp. 429–441, 1996.

[14] H. A. Kramers, "Théorie générale de la rotation paramagnétique dans les cristaux," *Proceedings of the Royal Academy of Sciences*, vol. 33, no. 9, pp. 959–972, 1930.